Background seismicity before and after the M_S7.8 Tangshan earthquake in 1976: Is its aftershock sequence still continuing?

Yue Liu[1,6]✉, Jiancang Zhuang [2,1,3,4,5,6], and Changsheng Jiang[5,6]✉

1. Institute of Earthquake Forecasting, Key Laboratory of Earthquake Prediction, China Earthquake Administration, 63 Fuxing Road, Haidian, Beijing 100036, China
2. The Institute of Statistical Mathematics, Research Organization of Information and Systems 10-3 Midori-cho, Tachikawa, Tokyo 190-8562, Japan
3. Department of Statistical Science, The University for Advanced Studies (SOKEN) 10-3 Midori-cho, Tachikawa, Tokyo 190-8562, Japan
4. London Mathematical Laboratory, 8 Margravine Gardens, Hammersmith, London W6 8RH, UK
5. Institute of Geophysics, China Earthquake Administration, No.5 Minzudaxue Nanlu, Haidian, Beijing 100081, China
6. China Seismic Experimental Site, China Earthquake Administration, 63 Fuxing Road, Haidian, Beijing 100036, China

Corresponding author: Yue Liu, liuyue@ief.ac.cn

Corresponding author: Changsheng Jiang, jiangcs@cea-igp.ac.cn

Key Points:

- The finite source ETAS model is applied to analyse the aftershock sequence of Tangshan M_S7.8 earthquake, China.
- The background seismicity of the Tangshan region has been lowered by the Tangshan mainshock.
- Aftershock sequence is still continuing but overridden by the background seismicity.

Abstract:

The aftershock zone of the 1976 M_S7.8 Tangshan earthquake, China, remains seismically active, experiencing moderate events such as the December 5th, 2019, M_S4.5 Fengnan event. It is still debated whether aftershock sequences following large earthquakes in low seismicity continental regions can persist for several centuries. To understand the current stage of the Tangshan aftershock sequence, we analyse the sequence record and separate background seismicity from the triggering effect using a finite-source epidemic-type aftershock sequence (FS-ETAS) model. Our results show that the background rate notably decreases after the mainshock. The estimated probability that the most recent M_S4.5 earthquake (December 5th, 2019, Fengnan District, Tangshan) is a background event is 63.8%. This indicates that the contemporary seismicity in the Tangshan aftershock zone can be characterised as a transition from aftershock activity to background seismicity. Although the aftershock sequence is still active in the Tangshan region, it is largely overridden by background seismicity.

Plain Language Summary

The 1976 M_S7.8 Tangshan earthquake occurred in the low seismicity continental region of North China Plain. The recurrence interval between successive earthquakes of similar magnitudes is more than 4,000 years. The recent M_S4.5 Fengnan earthquake (December 5th, 2019) struck the aftershock zone. It surged the debate on whether the aftershock sequence of Tangshan earthquake had ceased or was still active. To

understand the cotemporary seismicity of Tangshan region, we applied the finite-source epidemic-type aftershock sequence (FS-ETAS) model, in which rupture extensions were taken into consideration. The background seismicity was extracted from the catalogue. The results showed that the probability that the recent M_S4.5 event is triggered is approximately 40%, and that the background seismicity rate significantly decreased during the aftershock decay, comparing to that before the mainshock. We found that the background seismicity of the Tangshan region has been lowered by the Tangshan mainshock, and the aftershock sequence is still continuing but overridden by the background seismicity.

Keywords:

Tangshan earthquake; aftershock sequence; FS-ETAS model; background seismicity; rate-and-state dependent friction law; transition stage.

1 Introduction

Earthquake sequences have significant implications for understanding seismicity dynamics and in probabilistic seismic hazard assessments [*Toda and Stein*, 2018]. In particular, aftershock sequences following large intraplate earthquakes have longer durations and more complex spatiotemporal patterns than those following the mainshocks of similar magnitudes along plate boundaries. Some studies have found that aftershock sequence following large earthquakes in seismicity inactive continental regions can persist for a long time, although this assertion is still under debate.

Two methods are widely used in aftershock analysis, namely the Omori-Utsu law [*Utsu and Ogata*, 1995] and the method developed by *Dieterich* [1994] that incorporates stress changes on the fault to the rate-and-state dependent friction law. The Omori-Utsu formula is written as:

$$R(t) = K_0(t + c)^{-p}, \quad (1)$$

where R is the aftershock occurrence rate, t indicates the time after the mainshock, K_0 is dependent on the mainshock magnitude M, p is typically 0.8–1.2, and c is a case-dependent constant. For the rate-and-state dependent friction law, the aftershock decay is characterised as the original form of the Omori decay ($1/t$) and the aftershock duration time is derived as being proportional to the reciprocal of the shear stress rate:

$$t_a = \frac{a\sigma}{\dot{\tau}}, \quad (2)$$

where a is the constitutive parameter, σ is the normal stress, and $\dot{\tau}$ is the shear stressing rate [*Dieterich*, 1994].

Aftershock sequences are typically thought to last for no more than a decade [*Parsons*, 2002], however, it has been suggested that long-lasting aftershock sequences occur with complex patterns within continents [*Stein and Liu*, 2009]. This may be attributed to complicated fault networks [*M Liu and Stein*, 2016; *Valerio et al.*, 2017], slow loading rates [*Stein and Liu*, 2009], and crustal rheology [*Ziv*, 2006]. For example, using the model proposed by *Dieterich* [1994], it has been suggested that long-lasting aftershock activity dominates contemporary seismicity [*Stein and Liu*, 2009; *Toda and Stein*, 2018] in the New Madrid Fault Zone in the central United States. In contrast, a different view has been expressed based on research using the Epidemic Type Aftershock Sequence (ETAS) model [*Page and Hough*, 2014].

This debate also happens to seismicity following the M_S7.8 earthquake that occurred in Tangshan on July 28th 1976, where destructive earthquakes of a similar magnitude have a recurrence interval of more than 4,000 years [*Kang et al.*, 2013; *Ran and Wu*, 2019]. Since the 1976 earthquake, moderate seismic events ($M_S \geq 4$) have continued to occur in the aftershock zone and surrounding areas. *Liu and Wang* [2012], *Wang et al*. [2013], and *Zhong and Shi* [2012] suggest that the aftershock sequence of the Tangshan M_S7.8 earthquake would last for more than a hundred years based on their use of the model developed by *Dieterich* [1994]. They argue that the slow fault loading rate, which is estimated as less than 3mm/yr from either GPS data [*Wang et al.*, 2011]or repeating seismic events [*Li et al.*, 2007], is the cause of this long-term

aftershock decay. Nevertheless, *Jiang et al*. [2013] analyse the Tangshan sequence using the ETAS model [*Zhuang and Ogata*, 2006] and conclude that the recent events have a small probability of being triggered by previous ruptures, indicating that the aftershock seismicity has essentially ceased.

More recently, a M_S4.5 event occurred in the aftershock zone of the Tangshan main rupture on December 5th, 2019, named the Fengnan earthquake [http://www.ceic.ac.cn/], and has caught great concern in the public and also in Chinese seismologists. Whether this moderate earthquake occurred as a result of the long-lasting mainshock triggering effect or enhanced background seismicity is of critical concern for the analysis of earthquake risks in aftershock zones. To better understand the Tangshan aftershock sequence, here we apply the finite-source (FS) ETAS model [*Guo et al.*, 2019; *Guo et al.*, 2017] accounting for the rupture extension.

2 Tectonic setting and data

The 1976 M_S7.8 Tangshan earthquake is one of the most devastating intraplate earthquakes of the last 100 years, causing more than 240,000 deaths, 800,000 injuries, and largely destroying the city of Tangshan. It occurred on the hidden, active Tangshan Fault, which is a near-vertical NE trending right-lateral strike-slip fault in the eastern part of the North China Plain, buried under complex sedimentary basins in a relatively stable tectonic environment [*Chen et al.*, 1979; *Q Liu et al.*, 2007]. The rupture propagated bilaterally to a length of 84–140 km [*Huang and Tein Yeh*, 1997;

122 *Wan et al.*, 2008]. The orientation of the regional stress field displayed extensive
123 clockwise rotation before and after the earthquake, as determined from aftershock
124 data [*Xu and Wang*, 1986]. Contemporary strain accumulation in the Tangshan
125 earthquake source region revealed using Global Positioning System (GPS) datasets
126 [*Wu et al.*, 2016; *Zhang et al.*, 2018] is consistent with the China North Plain.

127 The datasets (http://www.chinarraydmc.cn/products/queryData?id=0) used in this
128 study are compiled by the China Earthquake Networks Center. Data for earthquakes
129 occurring within the region between 38° to 42°N and 115.5° to 120.5°E (Fig. 1a) and
130 within the depth range of 0–50 km are extracted. The study interval in the catalogue
131 extends from January 1th 1970 to December 5th, 2019. The magnitude threshold is set
132 at $M_L \geq 4.0$ due to the incomplete records for $M_L < 4$ events during a short period
133 after the mainshock (Fig. 1b). The number of events with a magnitude of $M \geq 4$ before
134 and after the mainshock is 22 and 1,072, respectively, and 188 and 2,033 as $M \geq 3.0$
135 events, respectively. The occurrence rate of $M \geq 4$ earthquakes before the mainshock
136 and since 2010 is 3.3 events/yr and 1.5 events/yr, respectively (Fig. 1c).

137 The occurrence times, locations, magnitudes, and depths of important events meeting
138 of interest in the study including the mainshock, M_S6.5+ aftershocks, and M_S4.5+
139 events within the past 10 years of the mainshock, are as follows:
140 (1) Tangshan mainshock, 1976-07-28 03:07:53, (118.18°E, 39.63°N), M_S7.8, 11 km
141 (2) Luanxian event I, 1976-07-28 18:45:33, (118.65°E, 39.83°N), M_S7.1, 10 km
142 (3) Ninghe event, 1976-11-15 21:53:02, (117.83°E, 39.40°N), M_S6.9, 17 km
143 (4) Luanxian event II, 2012-05-28 10:05:52, (118.47°E, 39.71°N), M_S4.7, 22 km

144 (5) Chaoyang event, 2016-5-22 17:08:06, (120.10°E, 41.62°N), M_S4.5, 6 km

145 (6) Fengnan event, 2019-12-05 08:12:29, (117.99°E, 39.33°N), M_S4.5, 7 km.

146 **3 Methodology**

147 The Epidemic Type Aftershock Sequence (ETAS) model, which accounts for
148 stationary background seismicity and secondary aftershocks, is developed by Ogata
149 (1988) based on the Omori-Utsu law [*Utsu and Ogata*, 1995]. The ETAS model has
150 been widely and successfully used to quantify the clustering patterns of seismicity
151 [e.g., *Helmstetter et al.*, 2006; *Lombardi et al.*, 2010; *Zhuang et al.*, 2018] with
152 space-time models being developed by incorporating both location and occurrence
153 time data [e.g., *Ogata*, 1998; *Zhuang and Ogata*, 2006; *Zhuang et al.*, 2002]. Recently,
154 the finite-source ETAS (FS-ETAS) model incorporating fault geometry and rupture
155 extensions is developed from the space-time ETAS model by *Guo et al*. [2017, 2019].
156 Compared with the traditional space-time point process models, the FS-ETAS model
157 shows better performance in clustering analysis. Therefore, we apply the FS-ETAS
158 model [*Zhuang et al.*, 2018] to analyse the ongoing seismicity in the Tangshan region.
159 We do not consider earthquake depth: each event is by default treated as being
160 independent of the other components.

161 In the FS-ETAS model, the conditional intensity function (time-varying seismicity
162 rate) can be written as follows:

$$\lambda(t,x,y) = \mu(x,y) + \sum_{i:t_i<t} \kappa(M_i) g(t-t_i) f(x,y;S_i,M_i). \quad (3)$$

The background rate μ is assumed to be variable in space but constant in time, and $\kappa(M_i)$ represents the magnitude-dependent intensity triggered by an event with the magnitude M_i and can be written as follows:

$$\kappa(M_i) = Ae^{\alpha(M_i - M_c)}, \tag{4}$$

where A and α are constants, and M_c is the completeness magnitude of the dataset. The normalized temporal probability density function (p.d.f.) is expressed as:

$$g(t) = \frac{p-1}{c}\left(a + \frac{t}{c}\right)^{-p}. \tag{5}$$

The spatial response kernels (p.d.f.) of major earthquakes containing rupture extensions are treated as finite sources, and other earthquakes are considered as point sources, thus:

$$f(x, y; S_i, M_i) = \begin{cases} \dfrac{q-1}{\pi D'^2} \dfrac{\iint_{S_i} \left[1 + \dfrac{(x-u)^2 + (y-v)^2}{D'^2}\right]^{-q} \tau_i(u,v)\,du\,dv}{\iint_{S_i} \tau_i(u,v)\,du\,dv}, & \text{if } S_i \text{ is a finite source} \\ \dfrac{q-1}{\pi D^2 e^{\gamma (M_i - M_C)}} \left[1 + \dfrac{(x-x_i)^2 + (y-y_i)^2}{D^2 e^{\gamma (M_i - M_C)}}\right]^{-q}, & \text{if } S_i = (x_i, y_i) \text{ is a point source} \end{cases} \tag{6}$$

where S_i is the projection on the earth surface of the rupture area of the ith event, $\tau_i(u, v)$ is the productivity density of directly triggered offspring at a location (u, v) in S_i, D', D, q and γ are constants.

For a given earthquake catalogue, the model parameters, the background rate, and the productivity densities can be estimated synchronically through an iterative algorithm with the combination of nonparametric estimation and maximizing likelihood estimation (MLE). Here we omit the details and refer to *Guo et al.* [2017, 2018] and *Zhuang et al*. [2018].

4 Data analysis

4.1 Computation setting

We first set 0.1 days after the mainshock as the start of the fitting time interval to avoid the influence of the missing aftershocks. The target space window for calculating the likelihood function is (38.5° to 41°N) × (116° to 120°E). Earthquakes in the dataset that do not fall within this range are complementary events, which contribute to the conditional intensity but not the likelihood function. Counting the triggering effect from these complementary events when computing the conditional intensity function is used to correct for the edge effect.

We use two schemes to establish the initial source zones for large earthquakes (Fig. 1) as follows: in Model 1, only the Tangshan mainshock is regarded as having a finite source, and in Model 2, two other events larger than M_S6.5 are also considered, namely the M_S7.1 Luanxian event (which occurs on the same day as the mainshock) and the M_S6.9 Ninghe earthquake (15th November, 1976). We select a relatively large region for each earthquake to ensure the entire range of the source zones are included. The estimates of productivity from the patches outside the source zones are near zero in the calculation output. Such an extension is aimed at achieving the best possible model of the off-fault aftershocks triggered by the stress changes. In Model 1, the fault rupture caused by the Tangshan sequence is entirely contained in the FS-model. In Model 2, the rupture extension is also related to the two large aftershocks. All of the source regions are divided into 0.02° × 0.02° grids.

4.2 Basic fitting results

The fitted model parameters and log-likelihood values are listed in Table 1. The higher likelihood values yielded from Model 1 asserts that it is a better model. Therefore, we focus the following discussion on the outputs of Model 1. Among the model parameters, α represents the difference in triggering ability between large and small events. In Table 1, a large value of α (approximately 1.9) implies that most of the triggered events are induced by a few large events. Parameter A represents the productivity of an event of magnitude M_c, and decreases from 0.49 in Model 1 to 0.46 in Model 2.

4.3 Productivity density pattern and rupture distribution

The rupture caused by the Tangshan sequence occurred mainly in three fault segments with different strike and dip angles, making the aftershock sequence temporally and spatially complex. We estimate the direct offspring productivity (Fig. 2) of each patch of the rupture plane of the mainshock and the two large aftershocks (i.e., Luanxian M_S7.1 and Ninghe M_S6.9) using the FS-ETAS model. The power of aftershock generation and the fault slip distribution are, as expected, complementary to each other. Patches with higher productivity density yield relatively smaller slip. Along the mainshock fault, the aftershock productivity density reaches a maximum of 1.5 events/patch at the northern tip of the fault, while the southern part is characterised by a relatively low productivity density and larger coseismic slip. Similar compensating

patterns in the productivity density and coseismic slip data are found for the Luanxian earthquake rupture.

4.4 Fengnan M_S4.5 event

The probability that the recent Fengnan M_S4.5 earthquake is a background event estimated by Models 1 and 2 is 63.8% and 55.4%, respectively. As such, the probability of the event having been triggered is approximately 40%. We also compare the correlations between the Fengnan event and the M_S6.5+ earthquakes in the dataset. This indicates that the probability of the Fengnan event having been triggered by the Tangshan mainshock and Ninghe M_S6.9 rupture is 15.1% and 1.2%, respectively, based on Model 1, and 20.8% and 11%, respectively, based on Model 2. These probabilities imply that background seismicity overrides aftershock activity in the contribution to the occurrence of the Fengnan event.

4.5 Background rate

Background events and triggered events are separated from the catalogue using a de-clustering method. When the background probabilities $\varphi_i = \mu(x_i, y_i)/\lambda(t_i, x_i, y_i)$ for each event *i* are determined, the cumulative background seismicity in region *R* can be estimated by summing the background probabilities for each event, as follows [*Zhuang et al.*, 2005]:

$$B(t) = \sum_{i:(x_i, y\_i)\in R} \varphi_i I(t_i < t), \tag{7}$$

where $I(\cdot)$ is equal to 1 when the statement is true or 0 when false.

For both of the models that we used, the average number of background events are consistent at 82.6 and 84.4 for Models 1 and 2, respectively. From the temporal variation in cumulative background seismicity (Fig. 3), we find that the background rate during the aftershock decay period transits to a significantly lower level than before the mainshock. The reduction in the background rate in this area can also be seen in Figure 1c.

5 Discussion

Background seismicity can be altered by large earthquakes, which can modify the seismic environment including fault properties, interactions between the lower crust and upper mantle, fault loading rates, and stress fields. To understand whether the background seismicity rate is changed by the mainshock of the Tangshan earthquake, we estimate the background rate before and after the event. As the beginning of the catalogue is 1970, only 6.6 years' data are available to estimate the background seismicity before the mainshock. During this period, only weak clustering is observed in the seismicity data, indicating that seismicity is consistent with the background level. As shown in Figure 1c, the post-shock seismicity decay has approximately followed the Omori-Utsu formula, reaching a level lower than the pre-mainshock background level. These findings are also confirmed by the FS-ETAS model results (Fig. 3).

Such a shift can be explained by the rate-and-state dependent friction law [*Dieterich*, 1994; *Toda et al.*, 2002]. Changes in stressing rate alters the seismicity rate. Whether

the seismicity is enhanced or reduced depends on whether the stressing rate increases or decreases, respectively, as illustrated in Figure 4. If the stressing rate on the nearby faults after the sudden stress drop caused by the mainshock remains the same as before, then, after the aftershock activity decays away, seismicity rate should go back to the background level same as the pre-shock period. In this study, the lowered background seismicity rate in the Tangshan aftershock zone after the mainshock indicates that the stressing rate has been lowered by the mainshock.

According to the analysis of the most recent M_S4.5 Fengnan event, we have shown that while the Tangshan aftershock sequence is still active, it is currently overridden by the background seismicity. As such, the seismicity of the Tangshan region represents a transition between aftershock activity and background seismicity. Our conclusion that the aftershock seismicity remains active in this region supports the results by *Liu and Wang* [2012] and *Wang et al*. [2013]. However, we have two points different from them: one is how long can the aftershock last, and the other is whether the background activity currently dominates. In estimating the aftershock duration using equation (2), *Liu and Wang* [2012] assume $a\sigma$ to be 0.15 MPa and conclude that aftershock activity could dominate the Tangshan aftershock zone for more than a century. However, the uncertainty in $a\sigma$ is large, in the order of 0.001–0.1 MPa [*Hainzl et al.*, 2009]. *Liu and Wang* [2012] and *Wang et al*. [2013] also state that the present-day seismicity rate is higher than before the mainshock based on records of $M_L \geq 3$ events. We suggest that pre-1976 events in the catalogue with magnitudes of

3.0 to 4.0 might not be completely recorded. Furthermore, based on our findings, background seismicity appears to dominate in this region over aftershock activity.

6. Conclusions

We analyse the Tangshan sequence using a FS-ETAS model that accounts for fault rupture extensions. We show that the background level of seismicity in the Tangshan region is, at present, lower than before the mainshock of the 1976 event, and the probability that the most recent M_S4.5 event is triggered by previous ruptures is approximately 40%. Thus, we conclude that contemporary seismicity in the Tangshan region represents a transition from aftershock-dominated to normal seismicity. Further research is now required to determine whether similar temporally dynamic seismicity patterns exist in other midcontinental regions.

Acknowledgments

We would like to thank the Institute of Geophysics, China Earthquake Administration for providing the catalogue data compiled by China Earthquake Networks Center, which are accessible online (http://www.chinarraydmc.cn/products/queryData?id=0). This study is supported by China Earthquake Science Experiment Project, CEA (grant Nos. 2019CSES0105, 2019CSES0106). YL is also partially supported by National Natural Science Foundation of China (Grant No. 41704093), the National Key R & D Program of China (Grant Nos. 2018YFE0109700, 2017YFC1500501), Institute of Earthquake Forecasting, CEA (Grant No, 2018IES0403), and CEA (Grant No. 2020020201). JZ is also partially supported by Grants-in-Aid no. 19H04073 for

Scientific Research from the Japan Society for the Promotion of Science (JSPS). We thank Yicun Guo from the University of Chinese Academy of Sciences, Professor Yongxian Zhang and Hui Wang from the Institute of Earthquake Forecasting, CEA, for their valuable discussions, and Jinmeng Bi from Tianjin Earthquake Agency for his assistance in data preparation.

References:

Chen, Y., B. Lin, X. Wang, L. Huang, and M. Liu (1979), A dislocation model of the Tangshan earthquake of 1976 from the inversion of geodetic data, *Chinese Journal of Geophysics. (in Chinese)*, *22*(3), 201-216.

Dieterich, J. (1994), A constitutive law for rate of earthquake production and its application to earthquake clustering, *Journal of Geophysical Research: Solid Earth*, *99*(B2), 2601-2618.

Guo, Y., J. Zhuang, and Y. Ogata (2019), Modeling and forecasting aftershocks can be improved by incorporating rupture geometry in the ETAS model, *Geophysical Research Letters*.

Guo, Y., J. Zhuang, N. Hirata, and S. Zhou (2017), Heterogeneity of direct aftershock productivity of the main shock rupture, *Journal of Geophysical Research: Solid Earth*, *122*(7), 5288-5305.

Hainzl, S., B. Enescu, M. Cocco, J. Woessner, F. Catalli, R. Wang, and F. Roth (2009), Aftershock modeling based on uncertain stress calculations, *Journal of Geophysical Research: Solid Earth*, *114*(B5).

Helmstetter, A., Y. Y. Kagan, and D. D. Jackson (2006), Comparison of short-term and time-independent earthquake forecast models for southern California, *Bulletin of the Seismological Society of America*, *96*(1), 90-106.

Huang, B.-S., and Y. Tein Yeh (1997), The fault ruptures of the 1976 Tangshan earthquake sequence inferred from coseismic crustal deformation, *Bulletin of the Seismological Society of America*, *87*(4), 1046-1057.

Kang, L., Q. Guosheng, C. Jianqiang, W. Weiguo, and N. Baokun (2013), Recurrence characteristics of major earthquakes in the Tangshan area, north China, *Acta Geologica Sinica‐English Edition*, *87*(1), 254-271.

Li, L., Q. F. Chen, X. Cheng, and F. Niu (2007), Spatial clustering and repeating of seismic events observed along the 1976 Tangshan fault, north China, *Geophysical Research Letters*, *34*(23).

Liu, M., and H. Wang (2012), Roaming earthquakes in China highlight midcontinental hazards, *Eos, Transactions American Geophysical Union*, *93*(45), 453-454.

Liu, M., and S. Stein (2016), Mid-continental earthquakes: Spatiotemporal occurrences, causes, and hazards, *Earth-Science Reviews*, *162*, 364-386.

Liu, Q., J. Wang, and J. Chen (2007), Seismogenic tectonic environment of 1976 great Tangshan earthquake: results given by dense seismic array observations, *Earth Science Frontiers (in Chinese)*, *14*(6), 0-0.

Lombardi, A. M., M. Cocco, and W. Marzocchi (2010), On the increase of background seismicity rate

during the 1997–1998 Umbria-Marche, Central Italy, sequence: apparent variation or fluid-driven triggering?, *Bulletin of the Seismological Society of America*, *100*(3), 1138-1152.

Ogata, Y. (1998), Space-time point-process models for earthquake occurrences, *Annals of the Institute of Statistical Mathematics*, *50*(2), 379-402.

Page, M. T., and S. E. Hough (2014), The New Madrid seismic zone: Not dead yet, *Science*, *343*(6172), 762-764.

Parsons, T. (2002), Global Omori law decay of triggered earthquakes: Large aftershocks outside the classical aftershock zone, *Journal of Geophysical Research: Solid Earth*, *107*(B9), ESE 9-1-ESE 9-20.

Ran, H., and G. Wu (2019), Seismicity around Late Quaternary Active Faults in China, *Bulletin of the Seismological Society of America*, *109*(4), 1498-1523.

Stein, S., and M. Liu (2009), Long aftershock sequences within continents and implications for earthquake hazard assessment, *Nature*, *462*(7269), 87.

Toda, S., and R. S. Stein (2018), Why aftershock duration matters for probabilistic seismic hazard assessment, *Bulletin of the Seismological Society of America*, *108*(3A), 1414-1426.

Toda, S., R. S. Stein, and T. Sagiya (2002), Evidence from the AD 2000 Izu islands earthquake swarm that stressing rate governs seismicity, *Nature*, *419*(6902), 58.

Utsu, T., and Y. Ogata (1995), The centenary of the Omori formula for a decay law of aftershock activity, *Journal of Physics of the Earth*, *43*(1), 1-33.

Valerio, E., P. Tizzani, E. Carminati, and C. Doglioni (2017), Longer aftershocks duration in extensional tectonic settings, *Scientific reports*, *7*(1), 16403.

Wan, Y., Z. Shen, G. Diao, F. Wang, X. Hu, and S. Sheng (2008), Rupture distribution of the 1976 Tangshan earthquake sequences inverted from geodetic data, *Chinese Journal of Geophysics. (in Chinese)*, *51*(3), 793-804.

Wang, H., M. Liu, J. Cao, X. Shen, and G. Zhang (2011), Slip rates and seismic moment deficits on major active faults in mainland China, *Journal of Geophysical Research: Solid Earth*, *116*(B2).

Wang, H., M. Liu, Z. Li, J. Cao, and Y. Jing (2013), Long Aftershock Sequences of Major Earthquakes in North China, *Earthquake (in Chinese)*, *33*(3), 1-12.

Wu, Y., L. Huang, C. Chen, S. Zhu, T. Jin, and X. Liu (2016), Coseismic and contemporary deformation features of the M_S7. 8 Tangshan earthquake in 1976, *Acta Seismologica Sinica (in Chinese)*, *38*(4), 609-617.

Xu, Z., and S. Wang (1986), A possible change in stress field orientation due to the 1976 Tangshan earthquake, *pure and applied geophysics*, *124*(4-5), 941-955.

Zhang, Y., W. Zheng, Y. Wang, D. Zhang, Y. Tian, M. Wang, Z. Zhang, and P. Zhang (2018), Contemporary deformation of the North China plain from Global Positioning System data, *Geophysical Research Letters*, *45*(4), 1851-1859.

Zhong, Q., and B. Shi (2012), Aftershock duration of the 1976 M_S7.8 Tangshan earthquake and implication for seismic hazaard aestimation, *Acta Seismologica Sinica*, *34*(4), 494-508.

Zhuang, J., and Y. Ogata (2006), Properties of the probability distribution associated with the largest event in an earthquake cluster and their implications to foreshocks, *Physical Review E*, *73*(4), 046134.

Zhuang, J., Y. Ogata, and D. Vere-Jones (2002), Stochastic declustering of space-time earthquake occurrences, *Journal of the American Statistical Association*, *97*(458), 369-380.

Zhuang, J., C. P. Chang, Y. Ogata, and Y. I. Chen (2005), A study on the background and clustering

seismicity in the Taiwan region by using point process models, *Journal of Geophysical Research: Solid Earth*, *110*(B5).

Zhuang, J., M. Murru, G. Falcone, and Y. Guo (2018), An extensive study of clustering features of seismicity in Italy from 2005 to 2016, *Geophysical Journal International*, *216*(1), 302-318.

Ziv, A. (2006), Does aftershock duration scale with mainshock size?, *Geophysical research letters*, *33*(17).

Figure captions:

Figure 1. (a) Locations of $M_L \geq 2.5$ earthquakes in the Tangshan and surrounding regions between January 1st, 1970, and December 5th, 2019. The blue dashed rectangle indicates the space window used in the likelihood function calculation. The black dashed polygons (1, 2, and 3) represent finite mainshock source areas of the Tangshan M_S7.8, Luanxian M_S7.1, and Ninghe M_S6.9 events, respectively. The yellow star and circle mark the epicentres of the Tangshan M_S7.8 event (1976) and the M_S4.5 Fengnan event (2019), respectively. Major faults in the region are shown as black lines [*Kang et al.*, 2013]; (b) Magnitude-time plot of $M_L \geq 2.5$ earthquakes in (a). The red rectangle indicates incomplete records; (c) Seismicity rates for $M \geq 4$ events in (a). The number of events per year is indicated by the circles.

Figure 2. Comparison between aftershock productivity density (black circles) and slip distribution (red circles, according to Wan et al., 2008) along the Tangshan mainshock rupture. The sizes of the black and red circles are proportional to the aftershock productivity density and slip sizes, respectively.

Figure 3. (a) Cumulative background seismicity (red curve), cumulative seismicity (black curve), and cumulative clustering seismicity (green curve) for Figure 1(a); (b) An enlarged view of the cumulative background seismicity. The blue dashed line shows the increasing rate of cumulative background events before the mainshock.

Figure 4. Illustrations of the relationship between the change in stressing rate and seismicity rate. The top panels show the response in seismicity rate when a sudden

411 stress drop occurs but the stressing rate remains the same as before the stress drop.
412 The middle panels show the transition of seismicity rate from its original to a new
413 level when the stressing rate is increased (red) or decreased (green). The bottom
414 panels show the corresponding responses in seismicity rate when the stressing rate
415 changes after a stress drop, red for increasing and green for decreasing.

416 Table 1. Estimated parameters from two FS-ETAS models fitted to the event
417 catalogue (1970-1-1 to 2019-12-5).

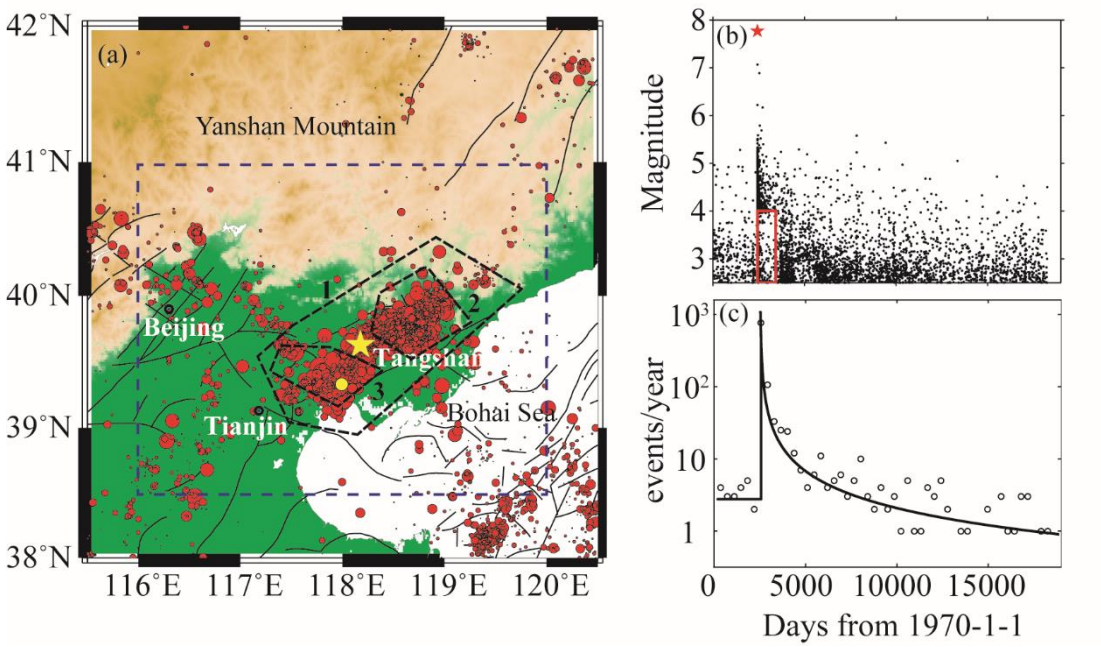

Figure 1. (a) Locations of $M_L \geq 2.5$ earthquakes in the Tangshan and surrounding regions between January 1st, 1970, and December 5th, 2019. The blue dashed rectangle indicates the space window used in the likelihood function calculation. The black dashed polygons (1, 2, and 3) represent finite mainshock source areas of the Tangshan M_S7.8, Luanxian M_S7.1, and Ninghe M_S6.9 events, respectively. The yellow star and circle mark the epicentres of the Tangshan M_S7.8 event (1976) and the M_S4.5 Fengnan event (2019), respectively. Major faults in the region are shown as black lines [*Kang et al.*, 2013]; (b) Magnitude-time plot of $M_L \geq 2.5$ earthquakes in (a). The red rectangle indicates incomplete records; (c) Seismicity rates for $M \geq 4$ events in (a). The number of events per year is indicated by the circles.

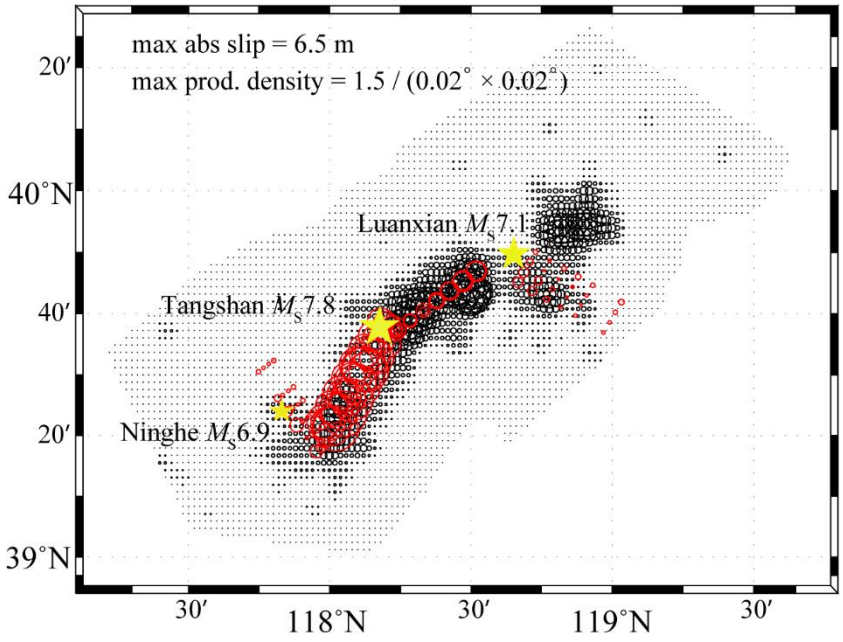

Figure 2. Comparison between aftershock productivity density (black circles) and slip distribution (red circles, according to Wan et al., 2008) along the Tangshan mainshock rupture. The sizes of the black and red circles are proportional to the aftershock productivity density and slip sizes, respectively.

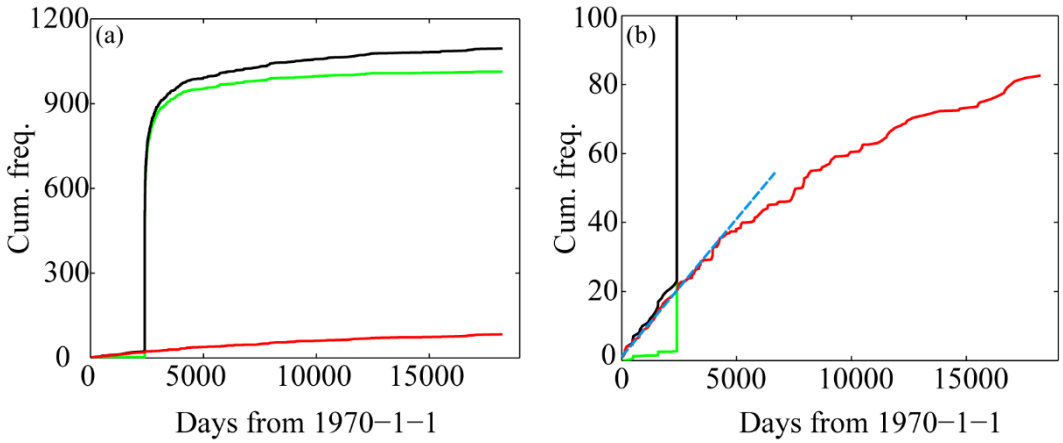

Figure 3. (a) Cumulative background seismicity (red curve), cumulative seismicity (black curve), and cumulative clustering seismicity (green curve) for Figure 1(a); (b) An enlarged view of the cumulative background seismicity. The blue dashed line shows the increasing rate of cumulative background events before the mainshock.

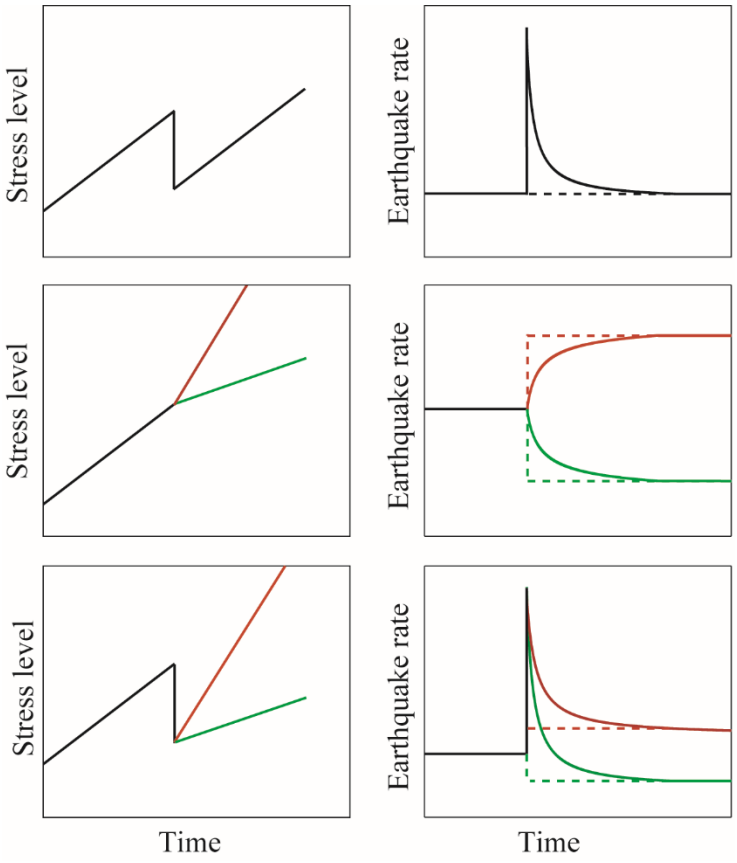

Figure 4. Illustrations of the relationship between the change in stressing rate and seismicity rate. The top panels show the response in seismicity rate when a sudden stress drop occurs but the stressing rate remains the same as before the stress drop. The middle panels show the transition of seismicity rate from its original to a new level when the stressing rate is increased (red) or decreased (green). The bottom panels show the corresponding responses in seismicity rate when the stressing rate changes after a stress drop, red for increasing and green for decreasing.

452 Table 1. Estimated parameters from two FS-ETAS models fitted to the event
453 catalogue (1970-1-1 to 2019-12-5).

Model	A	α	c (10^{-2}day)	p	D (10^{-5}deg^2)	q	γ	D'(10^{-5}deg^2)	log L
1	0.49	1.90	0.15	1.03	0.64	1.48	2.23	3.48	-2206
2	0.46	1.94	0.15	1.03	0.46	1.53	2.92	4.62	-2263

454

455